Vortex-ring mixing as a measure of diastolic function of the human heart: Phantom validation and initial observations in healthy volunteers and patients with heart failure.

Töger, Johannes; Kanski, Mikael; Arvidsson, Per; Carlsson, Marcus; Kovács, Sándor J; Borgquist, Rasmus; Revstedt, Johan; Söderlind, Gustaf; Arheden, Håkan; Heiberg, Einar

Published in:
Journal of Magnetic Resonance Imaging

DOI:
10.1002/jmri.25111

2016

Document Version:
Peer reviewed version (aka post-print)

Vortex-ring mixing as a measure of diastolic function of the human heart: phantom validation and initial observations in healthy volunteers and patients with heart failure

Johannes Töger PhD[1,2], Mikael Kanski MD PhD[1], Per M Arvidsson MD[1],

Marcus Carlsson MD PhD[1], Sándor J Kovács PhD MD[3], Rasmus Borgquist MD PhD[4],

Johan Revstedt PhD[5], Gustaf Söderlind PhD[2], Håkan Arheden MD PhD[1], Einar Heiberg PhD[1,2,6*]

[1]Department of Clinical Physiology, Lund University Hospital, Lund University, Lund, Sweden

[2]Department of Numerical Analysis, Centre for Mathematical Sciences, Lund University, Lund, Sweden

[3]Department of Internal Medicine, Cardiovascular Division, Washington University School of Medicine, St Louis, USA

[4]Department of Arrhythmias, Lund University Hospital, Lund, Lund University, Lund, Sweden

[5]Department of Energy Sciences, Faculty of Engineering, Lund University, Lund, Sweden

[6]Department of Biomedical Engineering, Faculty of Engineering, Lund University, Lund, Sweden

*: Corresponding author:

Einar Heiberg

Lund University, Department of Clinical Physiology

Lund University Hospital, SE-22185 Lund, Sweden

einar.heiberg@med.lu.se

Phone: +46-46-171605, Fax: +46-46-151769

Grant support

This study was supported by Swedish Research Council grants 621-2005-3129, 621-2008-2949 and K2009-65X-14599-07-3, National Visualization Program and Knowledge Foundation grant 2009-0080, the Medical Faculty, Lund University, Sweden, the Region of Scania, Sweden and the Swedish Heart-Lung Foundation. SJK received support from the Barnes-Jewish Hospital Foundation and The Alan A. and Edith L. Wolff Charitable Trust, St. Louis, MO, USA.

Running title

Vortex ring mixing in the left ventricle

ABSTRACT

Purpose

To present and validate a new method for 4D flow quantification of vortex-ring mixing during early, rapid filling of the left ventricle (LV) as a potential index of diastolic dysfunction and heart failure.

Materials and Methods

4D flow mixing measurements were validated using planar laser-induced fluorescence (PLIF) in a phantom setup. Controls (n=23) and heart failure patients (n=23) were studied using 4D flow at 1.5T (26 subjects) or 3T (20 subjects) to determine vortex volume (VV) and inflowing volume (VV_{inflow}). The volume mixed into the vortex-ring was quantified as $VV_{mix\text{-}in} = VV – VV_{inflow}$. The mixing ratio was defined as $MXR = VV_{mix\text{-}in}/VV$. Furthermore, we quantified the fraction of the end-systolic volume (ESV) mixed into the vortex-ring ($VV_{mix\text{-}in}/ESV$) and the fraction of the LV volume at diastasis (DV) occupied by the vortex-ring (VV/DV).

Results

PLIF validation of MXR showed fair agreement (R^2=0.45, mean±SD 1±6%). MXR was higher in patients compared to controls (28±11% vs 16±10%, $p<0.001$), while $VV_{mix\text{-}in}/ESV$ and VV/DV were lower in patients (10±6% vs 18±12%, $p<0.01$ and 25±8% vs 50±6%, $p<0.0001$).

Conclusion

Vortex-ring mixing can be quantified using 4D flow. The differences in mixing parameters observed between controls and patients motivate further investigation as indices of diastolic dysfunction.

Key words: 4D flow, diastolic dysfunction, heart failure, validation, planar laser-induced fluorescence

INTRODUCTION

Intracardiac flow patterns are closely connected to the shape and motion of the heart and may be a sensitive marker of cardiac health (1, 2). Left ventricular (LV) diastolic dysfunction is a condition with poor prognosis even in its mild form (3), and may appear as an isolated disease, as an early stage of other cardiac disease or in connection to systolic heart failure (4). Diastolic dysfunction leads to reduced cardiac performance, especially during physical activity as the time available for filling is significantly reduced (5). Diastolic function is commonly diagnosed using a combination of several imaging measures (6, 7), and the resulting classification may be ambiguous or inconclusive. Therefore, additional non-invasive quantitative measures are needed. Due to the diastolic suction of the LV (8) and the associated anatomy, a vortex-ring is generated downstream from the mitral valve during the early, rapid filling phase (9, 10). Recent studies indicate that vortex-ring formation reflects diastolic function and overall cardiac health (2, 11, 12). Experiments have shown that vortex-ring rotation generates mixing of the inflowing and surrounding fluid (13, 14). The mixing ratio (MXR), defined as the amount of surrounding fluid pulled into the vortex-ring divided by total vortex-ring volume, was found to be inversely correlated to the vortex formation ratio (VFR) (13, 14), a parameter connected to diastolic function (11, 12, 15). Therefore, quantification of vortex-ring mixing during early rapid filling of the LV may provide new insights into the physiology and pathophysiology of diastole.

Mixing of blood in the LV vortex-ring may also affect rinsing of the endocardium to reduce the risk of thrombus formation.

Therefore, this paper aims to 1) present a new method for quantification of mixing ratio in the diastolic vortex-ring in the human left ventricle, 2) validate the method in vitro, and 3) investigate vortex-ring mixing in healthy controls and patients with congestive heart failure.

MATERIALS AND METHODS

PLIF Imaging of Phantom

A previously described vortex-ring flow phantom was used for validation (16) (Figure 1). The phantom setup has previously been used to validate velocity and vortex-ring volume (VV) measurements, and is extended here to validation of vortex-ring mixing. Five pump settings were used, with pulse volumes between 12 and 37 ml and peak nozzle velocities between 21 and 37 cm/s. One series of experiments was conducted with water, with Reynolds numbers ranging from 5200 to 8900. A second series of experiments was performed using a water-glycerine mixture as previously described (16) to investigate if higher fluid viscosity and increased temporal and spatial resolution would influence mixing quantification. As a consequence of increasing the viscosity to match the viscosity of blood, the Reynolds numbers in the water-glycerine experiments were lower compared to the water experiments (1800-2900). Planar laser-induced fluorescence (PLIF) flow visualization (Figure 1c) was performed using a LaVision flow imaging system (Göttingen, Germany) as previously described (16).

Quantification of MXR in PLIF Images

PLIF images were manually delineated to quantify vortex-ring volume (VV) (Figure 2). Inhomogeneous illumination was corrected by subtracting a second-order polynomial fit to background regions. An image histogram was computed and smoothed using a Gaussian filter. The minimum between the last and second-to-last peaks was used to determine the threshold between black and white pixels. Axial symmetry of the vortex-ring was assumed (14). While axial symmetry cannot be assumed in vivo, this assumption was used for the phantom validation due to the use of a 2D PLIF imaging system. Each pixel p in the image contributed a volume

$$V_p = \pi r_p \Delta x \Delta y, \qquad \text{[Eq. 1]}$$

where r_p is the vertical distance to the symmetry line (Figure 2b, green dashed line), and Δx and Δy are the pixel spacings. Vortex-ring volume (VV) was computed as the sum of the volume contributions from each pixel. Inflowing volume (VV_{inflow}) and mixed-in volume ($VV_{mix\text{-}in}$) were computed as the contributions of black and white pixels respectively.

MR Imaging of Phantom

Magnetic resonance (MR) imaging was performed on a 1.5T Philips Achieva MR scanner using a 32-channel cardiac coil (Philips Healthcare, Best, The Netherlands) as previously described (16).

4D Flow: 4D flow was performed using a three-dimensional phase contrast sequence (17, 18). Sequence parameters were based on previous in vivo scans from our lab (18) as follows: acquired matrix 64×62×40; acquired time phases 21; voxel size 3×3×3 mm; reconstructed matrix 80×80×40; reconstructed time phases 40; flip angle 8°; TR/TE 6.3/3.7 ms; VENC 100 cm/s; temporal resolution 50 ms; SENSE=2 and segmentation factor 2, acquisition time 16 minutes. Retrospective triggering to the pump trigger signal was used.

4D flow for glycerine experiments: A second series of experiments was performed using a water-glycerine mixture as previously described (16) to investigate if fluid viscosity and temporal and spatial resolution would influence mixing quantification. MR sequence parameters were as follows: acquired and reconstructed matrix 128×128×15; sagittal slices; acquired time phases 35; voxel size 1.5×1.5×3 mm; reconstructed time phases 35; flip angle 8°; TR/TE 7.5/4.7 ms; temporal resolution 30 ms; SENSE=2, no temporal segmentation, acquisition time 22 minutes. The VENC was reduced to 50 cm/s to increase the velocity signal-to-noise ratio.

Study Population and In Vivo MR Protocol

Controls (n=23) and patients with congestive heart failure (n=23) were included. All controls had blood pressure ≤140/90 mmHg, normal ECG and no history of cardiovascular disease. The study was approved by the regional ethical committee. All subjects provided written informed consent. All subjects underwent cardiac magnetic resonance (MR) at 1.5T (18 patients, 8 volunteers plus 6 volunteers for scan-rescan analysis) or 3T (5 patients, 15 volunteers) (Philips Achieva, Philips Healthcare, Best, The Netherlands). Subject demographics are shown in Tables 1 and 2. Imaging included balanced steady-state free precession (bSSFP) cine images in long-axis and short-axis views and 2D flow in the aorta as previously described (18). Presence of LV thrombus was assessed in MR images according to clinical routine.

Furthermore, 4D flow was performed at rest using a previously validated (16, 18) three-dimensional sequence (17). Scan parameters: spatial resolution 3×3×3 mm, flip angle 8°, TR/TE 6.3/3.7 ms, VENC 100 cm/s, temporal resolution 50 ms, SENSE=2 and segmentation factor 2. Retrospective ECG triggering was used. In all controls and 4 patients, respiratory gating was used. In 19 patients, respiratory gating was omitted to reduce scan time. In 8 controls, 4D flow was performed with and without respiratory gating in the same session. Furthermore, 6 healthy volunteers were scanned at 1.5T and 3T on the same day in random order. Alignment of cine and 4D flow images was assessed visually and manually adjusted when needed.

Phase Background Correction of 4D Flow Data

Concomitant gradient effects were compensated by the MR scanner (Maxwell correction). Residual phase background effects were corrected using one of the two following methods:

A) *Polynomial fit to stationary voxels:* Stationary voxels were automatically detected, and a first-order polynomial fit to velocities in stationary voxels. The computed polynomial was then subtracted from the whole 4D flow volume.

B) *Stationary scan (phantom measurements):* The pump was switched off and the tank left to settle for at least 20 minutes and 4D flow was then acquired in the tank. To avoid phase background drift due to gradient coil temperature variation (19), other MR sequences were run for 5 minutes before starting the stationary 4D flow sequence. A first-order polynomial was fit to all voxels in the stationary measurement. The computed polynomial was then subtracted from each dataset.

For all *in vivo* scans, the polynomial fit method (A) was used. Phantom data was evaluated using both methods separately.

Vortex-Ring Detection Using Lagrangian Coherent Structures

Lagrangian Coherent Structures (LCS) is a new method for flow analysis, enabling delineation of vortex-ring boundaries (20). LCS were generated as previously described (9) and validated (16). Briefly, the steps are as follows:

1) For each image plane and time phase, a grid of particles with 0.8 mm spacing was considered. To generate a flow map, each particle was traced backwards in time to the start of diastole using a fourth-order Runge-Kutta method with time step 5 ms. Hence, the LCS capture the history of the flow, from onset of diastole until the end of rapid filling. Linear interpolation of velocities was used in time and space for computing particle traces.

2) The Jacobian of the flow map in each grid point was computed using centered finite differences with neighboring grid points.

3) The finite-time Lyapunov exponent (FTLE) was computed as the logarithm of the norm of the Jacobian of the flow map.

Steps 1-3 were performed in the 2-, 3-, and 4-chamber long-axis views and in short-axis planes covering the whole LV. All views vere planned according to current guidelines for cardiac magnetic resonance (21). FTLE values were normalized to the 95^{th} percentile of FTLE values in the images in each time phase. Lines with FTLE values higher than 50% of this value were considered as LCS.

LCS images were generated for blood flow between the onset of diastole and the end of rapid filling. The onset of diastole (end-systole) was defined as the time of smallest LV blood volume in short-axis cine images. Figure 3 shows how the end of rapid filling was determined. The vortex-ring boundary was then delineated manually in short-axis slices, guided by delineations of the boundary in long-axis images (Figure 4).

Mixing Quantification

Mixing was quantified using two different methods as follows.

MXR Method 1

1) The origin of each voxel of blood within the vortex-ring at the end of rapid filling was computed using particle tracing, using a fourth-order Runge-Kutta method with time step 5 ms, backwards in time to the start of diastole. The boundary between the LV and left atrium was defined as a short-axis plane on the same level as the atrioventricular plane (or nozzle in the phantom experiments), located using long-axis cine images.

2) The vortex-ring volume (VV) was decomposed into two parts depending on the origin of each voxel of blood (Figure 4, right column):

I) *Inflowing blood – VV_{inflow}:* Voxels of blood in the vortex-ring originating from the atrial side of the mitral valve at end-systole.

II) *Mixed-in blood – $VV_{mix\text{-}in}$:* Voxels of blood in the vortex-ring originating from the ventricular side of the mitral valve at end-systole.

MXR Method 2

For method 2, VV was measured using delineation of LCS, and VV_{inflow} was measured by analyzing mitral valve flow as follows. First, a short-axis plane was chosen near the mitral valve (or at the end of the nozzle in water tank experiments). Through-plane flow was then reconstructed from the 4D flow data, and the transmitral flow was manually delineated. $VV_{mix\text{-}in}$ was then computed as $VV_{mix\text{-}in}=VV-VV_{inflow}$.

Definition of quantitative mixing parameters

Mixing ratio (MXR) was defined as $MXR=VV_{mix\text{-}in}/VV$. The fraction of the end-systolic volume (ESV) mixed into the vortex-ring was computed as $VV_{mix\text{-}in}/ESV$. The fraction of the LV diastatic volume (DV) involved in vortex-ring formation was computed as VV/DV (9).

In Vivo Interobserver and Interstudy Variability

Two observers (JT and PA, 4 and 2 years experience with LCS and mitral valve flow delineations respectively) delineated vortex-ring LCS and measured mitral valve flow independently in all subjects. Furthermore, one observer (JT) performed the analysis on data from 1.5T and 3T (n=6) and data with and without respiratory gating (n=8) to assess interstudy variability.

Vortex Formation Ratio

Vortex formation ratio (VFR), (stroke ratio, L/D, or vortex formation time, VFT), is a dimensionless measure of vortex-ring formation (2, 11, 15). VFR was computed using the established formula (2, 9, 22):

$$\mathrm{VFR} = \frac{4}{\pi} \times \frac{\mathrm{EWV}}{\mathrm{SV}} \times \frac{\mathrm{EDV}}{D^3} \times \mathrm{EF} = \frac{4}{\pi} \times \frac{\mathrm{EWV}}{D^3} \qquad \text{[Eq. 2]}$$

The E-wave volume (EWV) was computed by reconstructing transmitral flow from 4D flow data ($EWV=VV_{inflow}$ by method 2). Mitral valve diameter (D) was computed as the average of two measurements D_1 and D_2, where D_1 is the maximal distance between the mitral valve leaflet tips during rapid filling measured in the 3-chamber view, and D_2 is measured perpendicular to D_1 in short-axis images.

LV Volume Delineations

LV end-systolic volume (ESV), end-diastolic volume (EDV) and diastatic volume (DV, Figure 3) were determined by manual delineation of the endocardium in short-axis slices covering the LV, excluding papillary muscles. E-wave volume from the cine images (EWV_{Cine}) was computed as DV-ESV (Figure 3).

Mitral regurgitation was computed as the difference between short-axis SV and outflow measured by 2D-flow in the aorta. Mitral regurgitation fraction was computed as mitral regurgitation divided by SV.

Echocardiography and Clinical Measures

In 22 of 23 patients, echocardiography was performed using a standard imaging system (Vivid E9, GE Medical, Horten, Norway). Analysis was performed using Echopac software (Echopac BT12, GE Medical, Horten, Norway) by an experienced observer (RB, 10 years experience).

E/A, E/e' and E-wave deceleration time (DT) were measured according to current guidelines (23). The time between echocardiography and MR examinations was 85±130 days.

In 17 of 23 patients, 6-minute walk test (6MWT) was performed according to current guidelines (24).

Diastolic Function

Diastolic function was classified from MR data using the measures E/A, E/e', mean e', peak left atrial volume normalized to body surface area (BSA), mitral E-wave deceleration time (MDT), and pulmonary venous flow profile. E, A and pulmonary venous flow was extracted from 4D flow and e' was measured in the 4-chamber view. Left atrial volume was delineated in short-axis images. Diastolic function was then classified as impaired relaxation, pseudonormal or restrictive filling (23).

Statistical Analysis

Bias between measurements was computed using Bland-Altman analysis. Differences between observers and examinations were analyzed using paired t-tests. Differences between controls and patients, and between patient subgroups were analyzed using unpaired t-tests. Comparison of mixing between diastolic dysfunction classes was performed using one-way ANOVA. Differences with p-values <0.05 were considered statistically significant. Group values are given as mean±SD. Gender distribution in controls and patients was analyzed using Fisher's exact test. The ability of mixing measures and LV ejection fraction (EF) to distinguish between controls and patients was quantified using ROC analysis. Statistical analysis was performed using GraphPad Prism 6 (GraphPad Software, La Jolla, USA).

Power analysis for comparison of MXR between groups was performed as follows. Previous *in vitro* studies show that MXR varies between 0-40% (13, 14). We therefore aimed to detect a

difference of 10% at the α=0.05 confidence level. The SD within groups was assumed to be 10%, i.e. approximately twice the SD in the phantom validation to account for additional in vivo variation. This gives a minimum group size of n=17 for 80% power and n=22 for 90% power.

RESULTS

Accuracy and Precision

Figure 5 shows PLIF validation results for MXR for water and glycerine experiments. Method 1 shows poor agreement (bias 13±45%) and was therefore not considered useful, while Method 2 has acceptable performance (phase background correction method A: bias 6±14%, method B: 1±11%). For Method 2, Table 3 shows *in vivo* interobserver variability in controls (MXR: -4±8%, $VV_{mix\text{-}in}$/ESV: -5±10%, VV/DV: -2±5%) and patients (MXR: -5±9%, $VV_{mix\text{-}in}$/ESV: -2±4%, VV/DV: -2±7%), interstudy variability (MXR: 7±6%, $VV_{mix\text{-}in}$/ESV: 8±6%, VV/DV: 1±7%) and comparison of 4D flow with and without respiratory gating (MXR: -9±11%, $VV_{mix\text{-}in}$/ESV: -9±12%, VV/DV: -2±6%).The corresponding Bland-Altman plots are shown in Supporting Files 1-4.

In Vivo Results

Tables 1 and 2 show subject characteristics, LV volumes and VFR measurements. Acquisition time was 28±7 min in controls and 41±18 min in patients (p=0.002). Figure 4 shows a visualization of the developed method, demonstrating blood flow into the LV during rapid filling in one control and one patient with heart failure, using Volume Tracking (25) and LCS. The atrial blood flowing into the LV (red) forms an asymmetric toroidal vortex-ring and mixes with ventricular blood (blue). Supporting Files 5 and 6 show animated versions of Figure 4.

Figure 6 and Table 3 shows mixing measures in controls and patients. MXR was smaller in controls compared to patients (16±10 vs 28±11%, $p<0.001$). Furthermore, $VV_{mix\text{-}in}$/ESV was larger in controls than in patients (18±12 vs 10±6%, $p<0.01$) and VV/DV was larger in controls than in patients (50±6 vs 25±8%, $p<0.0001$). There was no difference in mixing parameters between groups of patients with different class of diastolic dysfunction (Figure 6). There was no difference in VV between controls and patients (78±18 vs 79±26 ml, $p=0.96$), but statistically significant differences were found for both VV_{inflow} (65±13 vs 54±15 ml, $p=0.027$) and $VV_{mix\text{-}in}$ (13±10 vs 24±14 ml, $p=0.012$).

One control had insufficient image quality for measuring mitral valve diameter and was excluded from VFR and mitral valve diameter analysis. One control and two patients had insufficient three-chamber image quality and therefore D_1 and D_2 were both measured in short-axis images.

Linear regression between MXR and VFR showed a positive correlation in patients ($y=4.3x+14.7$, $R^2=0.38$, $p=0.002$), but no correlation in healthy volunteers ($R^2=0.07$, $p = 0.25$). There was no difference in mixing measures between patients with ischemic heart disease compared to dilated/non-ischemic heart disease (MXR: ischemic 27±12% vs dilated 31±10%, $p=0.39$; $VV_{mix\text{-}in}$/ESV: 9±6% vs 11±7%, $p=0.46$; VV/DV: 24±7% vs 26±10%, $p=0.72$). Figure 7 shows the relation between peak inflow velocity and MXR ($R^2=0.21$, $p=0.028$).

ROC curves for EF and mixing measures are shown in Supporting File 7. For EF and VV/DV, complete separation of the control and patient group were achieved (EF threshold: 45%, VV/DV threshold: 38%). For MXR, high sensitivity and specificity were found (threshold: 24%, sensitivity: 0.70, specificity: 0.83, area under curve (AUC): 0.80±0.07, $p<0.001$). For $VV_{mix\text{-}in}$/ESV, high sensitivity and poor specificity were found (threshold: 17%, sensitivity: 0.87, specificity: 0.52, AUC: 0.70±0.08, $p=0.021$).

Thrombus in the LV was found at MR examination in 3 of 23 patients (13%). There was no difference between patients with and without LV thrombus for MXR (24±7% vs 29±12%, p=0.61) $VV_{mix\text{-}in}$/ESV (5±3% vs 10±7%, p=0.45) or VV/DV (16±6% vs 26±8%, p=0.95).

Supporting File 8 shows the correlation of mixing measures versus quantitative echocardiography parameters (E/A, E/e' and DT) and 6MWT. No statistically significant correlations were found.

DISCUSSION

This study presents a new method for quantification of mixing of atrial and ventricular blood in the vortex-ring formed during early rapid filling of the LV (echocardiographic Doppler E-wave) using 4D flow and Lagrangian Coherent Structures. Validation of the method showed fair agreement between MR 4D flow and planar laser-induced fluorescence (PLIF). The differences in mixing between controls and patients suggest that mixing quantification may be used to increase our understanding of LV diastolic function and dysfunction.

PLIF validation shows that MXR can be quantified using 4D flow, with better agreement for background correction with stationary reference scan. The different results for the two background correction methods highlight the importance of phase background correction in 4D flow. MXR based on particle tracing showed poor agreement with PLIF, which can be explained by the failure of 4D flow to capture the 'winding' of the vortex-ring core (16). This reinforces the necessity of careful validation of quantitative 4D flow measures.

The phantom was designed to imitate in vivo vortex-ring formation as closely as possible. Although *in vivo* vortex-rings are asymmetric, symmetric vortex-rings were used to produce a repeatable experiment (9, 26, 27). Design issues limited the phantom to somewhat lower stroke

volumes and peak velocities than observed in vivo. However, mixing quantification can be expected to be more challenging in smaller vortex-rings, and the present results show that mixing can be measured in vortex-rings that are smaller than in vivo.

Fair interobserver and interstudy variability were found. However, larger differences were found for scans with and without respiratory gating, which must be taken into account when interpreting results as controls were scanned with respiratory gating and a majority of patients without. Therefore, the lower $VV_{mix\text{-}in}$/ESV in patients compared to controls may be due to differences in respiratory gating. However, MXR was higher in patients compared to controls, even though MXR was lower when not using respiratory gating. This suggests that the difference in MXR may be even bigger when scanning both patients and controls with our without respiratory gating. Consistent use of respiratory gating is preferable in future studies.

The difference in MXR between controls and patients may be connected to impaired diastolic function in patients. Specifically, LV diastolic suction of blood which drives normal LV filling (8, 28–30) is reduced in heart failure (31). Impaired suction and the compensatory increases in atrial contraction and left atrial filling pressure may be related to the higher in MXR in patients. We found no differences in mixing parameters with respect to diastolic function. In light of the variability of mixing measurements, a larger number of patients in each diastolic function class is needed to detect a physiological difference. However, the correlation between MXR and peak E-wave velocity suggests a connection between MXR and diastolic function, since increased E-wave velocity is common in restrictive diastolic dysfunction. No conclusions can be drawn from the absence of correlation between mixing measures and echocardiographic parameters due to the long time between MR and echocardiography.

MXR and $VV_{mix\text{-}in}$/ESV showed good performance for separating controls from patients. This suggests that mixing measures may be useful to identify disease in situations where echocardiography or other clinical measures are inconclusive. In the present population, EF separates controls and patients completely, which is explained by the fact that patients were recruited from another study where low EF was an inclusion criterion. This also explains the result that VV/DV separates controls and patients completely, since DV is a measure of LV volume, and all patients had pathologically enlarged LVs.

The difference in VV/DV between controls and patients confirms previous results on LV vortex-ring formation (9). The low VV/DV in patients shows that a smaller fraction of LV blood is involved in diastolic vortex-ring formation, which we hypothesize may lead to a higher risk of thrombus formation. Since few patients in this study presented with LV thrombus, a larger patient cohort is needed to test this hypothesis.

In this study, mixing is quantified during early, rapid filling of the LV. Previous studies have investigated mixing of blood over the whole heartbeat using saline dilution techniques (32) and computational modelling (33), showing that mixing of LV blood is incomplete over one heartbeat. The low $VV_{mix\text{-}in}$/ESV observed here reinforces the view that LV blood mixing is incomplete at rest.

The positive correlation between MXR and VFR in patients and lack of correlation in controls is in contrast to the strong negative correlation observed in water tank experiments (13, 14). Furthermore, Müller and Didden (13) predicted that MXR would approach zero at the transition from vortex-ring to a turbulent jet, later observed by Gharib *et al.* (15) to occur at an ‘optimal’ VFR close to 4. This suggests that an LV operating close to the optimal VFR would have an

MXR close to zero. In contrast, we observed an MXR of 16% in controls, and even higher (28%) in congestive heart failure patients, which may be explained by additional asymmetry and complexity of *in vivo* vortex-ring formation (9, 34, 35), the proximity of the endocardial wall and papillary muscles to the vortex-ring boundary (9, 36), and variations in inflow velocity profile (14).

The present study has some limitations. The 4D flow technique has limited spatial and temporal resolution and averages thousands of heartbeats. As a consequence, recurrent flow features are retained, while beat-to-beat variations are masked. Therefore, mixing values presented here may be seen as a lower limit. The presented method is limited by interobserver and interstudy variability. Improved imaging and post-processing is needed to enable clinical use of vortex-ring parameters.

Age and gender-matched controls were not included. Therefore, the present results serve mainly to demonstrate that mixing measurements can detect the known difference in diastolic function between healthy controls and heart failure patients.

Backward-time LCS were used to detect the leading edge of the vortex-ring. While the trailing edge of the vortex-ring can be identified using forward-time LCS in water tank experiments (37), this is not possible in vivo (9). Therefore, the leading edge of the vortex-ring was extrapolated to the atrioventricular plane (Figure 4, middle column).

In conclusion, the phantom validation, interobserver and interstudy variability shows that vortex-ring mixing during LV rapid filling can be quantified using 4D flow MR with fair accuracy and precision. The differences observed between healthy controls and patients with heart failure

justify further investigation of mixing parameters as markers of diastolic dysfunction and heart failure.

LIST OF ABBREVIATIONS

4D flow	Three-dimensional, time-resolved, three-directional phase contrast magnetic resonance velocity mapping (3D+time = 4D)
bSSFP	Balanced steady-state free precession
D	Mitral valve diameter
DV	Diastatic volume (Figure 3)
ECG	Electrocardiogram
EDV	End-diastolic volume (Figure 3)
EF	Ejection fraction
ESV	End-systolic volume (Figure 3)
EWV	E-wave volume (Figure 3)
FTLE	Finite-time Lyapunov Exponent, quantity computed from 4D flow data for LCS detection
LCS	Lagrangian coherent structures, a method for analysis of vortex-ring formation and pulsatile flow
LV	Left ventricle
MXR	Vortex-ring mixing ratio
PLIF	Planar laser-induced fluorescence, a laser method for flow visualization
VFR	Vortex formation ratio (Eq. 2). Also called VFT or L/D.
VV	Vortex-ring volume
$VV_{mix\text{-}in}$	The part of VV consisting of surrounding fluid mixed into the vortex-ring
VV_{inflow}	The part of VV consisting of inflowing fluid

SUPPORTING INFORMATION

Supporting File 1: Bland-Altman plots for interobserver variability in controls (Table 3).

Supporting File 2: Bland-Altman plots for interobserver variability in patients with heart failure (Table 3).

Supporting File 3: Bland-Altman plots for interstudy variability between 1.5T and 3T (Table 3).

Supporting File 4: Bland-Altman plots for difference between scans with and without respiratory gating (Table 3).

Supporting File 5: Volume Tracking animation of vortex-ring formation during rapid filling of the LV in one control (Figure 4).

Supporting File 6: Volume Tracking animation of vortex-ring formation during rapid filling of the LV in a patient with heart failure (Figure 4).

Supporting File 7: Receiver operating characteristic (ROC) curves for identifying patients from controls using EF, MXR, $VV_{mix\text{-}in}$/ESV and VV/DV.

Supporting File 8: Correlation of mixing measures (MXR, $VV_{mix\text{-}in}$/ESV, VV/DV) versus echo (E/e', E/A, DT) and 6MWT.

ACKNOWLEDGMENTS

EH is founder of Medviso AB, manufacturer of the image analysis software Segment. Ann-Helen Arvidsson, Christel Carlander, Reza Farazdaghi, Johanna Koul and Lotta Åkesson at the Department of Clinical Physiology, Lund University Hospital, Lund, Sweden are acknowledged for assistance in data collection. Tomas Hajdu at the Department of Medical Technology, Skåne University Hospital Lund, Sweden is acknowledged for design and construction of the phantom equipment.

REFERENCES

1. Föll D, Taeger S, Bode C, Jung B, Markl M: Age, gender, blood pressure, and ventricular geometry influence normal 3D blood flow characteristics in the left heart. *Eur Heart J Cardiovasc Imaging* 2013; 14:366–73.

2. Gharib M, Rambod E, Kheradvar A, Sahn DJ, Dabiri JO: Optimal vortex formation as an index of cardiac health. *Proc Natl Acad Sci U S A* 2006; 103:6305–8.

3. Redfield MM, Jacobsen SJ, Burnett JC, Mahoney DW, Bailey KR, Rodeheffer RJ: Burden of Systolic and Diastolic Ventricular Dysfunction in the Community. *Intern Med* 2003; 289:194–202.

4. Yancy CW, Jessup M, Bozkurt B, et al.: 2013 ACCF/AHA guideline for the management of heart failure: Executive summary: A report of the American college of cardiology foundation/American Heart Association task force on practice guidelines. *Circulation* 2013; 128:1810–1852.

5. Chung CS, Karamanoglu M, Kovács SJ, Kovacs SJ: Duration of diastole and its phases as a function of heart rate during supine bicycle exercise. *Am J Physiol Heart Circ Physiol* 2004; 287:2003–2008.

6. McMurray JJ V, Adamopoulos S, Anker SD, et al.: ESC Guidelines for the diagnosis and treatment of acute and chronic heart failure 2012. *Eur J Heart Fail* 2012:803–869.

7. Flachskampf FA, Biering-Sørensen T, Solomon SD, Duvernoy O, Bjerner T, Smiseth OA: Cardiac Imaging to Evaluate Left Ventricular Diastolic Function. *JACC Cardiovasc Imaging* 2015; 8:1071–1093.

8. Brecher GA: Experimental Evidence of Ventricular Diastolic Suction. *Circ Res* 1956; 4:513–518.

9. Töger J, Kanski M, Carlsson M, et al.: Vortex ring formation in the left ventricle of the heart: analysis by 4D flow MRI and Lagrangian coherent structures. *Ann Biomed Eng* 2012; 40:2652–62.

10. Falahatpisheh A, Pahlevan NM, Kheradvar A: Effect of the Mitral Valve's Anterior Leaflet on Axisymmetry of Transmitral Vortex Ring. *Ann Biomed Eng* 2015; 43:2349–2360.

11. Poh KK, Lee LC, Shen L, et al.: Left ventricular fluid dynamics in heart failure: echocardiographic measurement and utilities of vortex formation time. *Eur Heart J Cardiovasc Imaging* 2012; 13:385–93.

12. Ghosh E, Kovács SJ: The vortex formation time to diastolic function relation: assessment of pseudonormalized versus normal filling. *Physiol Rep* 2013; 1:e00170.

13. Müller EA, Didden N: Zur Erzeugung der Zirkulation bei der Bildung eines Ringwirbels an einer Düsenmündung. *Strojnícky Cas* 1980; 31:363–372.

14. Olcay AB, Krueger PS: Measurement of ambient fluid entrainment during laminar vortex ring formation. *Exp Fluids* 2008; 44:235–247.

15. Gharib M, Rambod E, Shariff K: A universal time scale for vortex ring formation. *J Fluid Mech* 1998; 360:121–140.

16. Töger J, Bidhult S, Revstedt J, Carlsson M, Arheden H, Heiberg E: Independent validation of four-dimensional flow MR velocities and vortex ring volume using particle imaging velocimetry and planar laser-Induced fluorescence. *Magn Reson Med* 2015. doi:10.1002/mrm.25683

17. Dyverfeldt P, Kvitting J-PE, Sigfridsson A, Engvall J, Bolger AF, Ebbers T: Assessment of fluctuating velocities in disturbed cardiovascular blood flow: In vivo feasibility of generalized phase-contrast MRI. *J Magn Reson Imaging* 2008; 28:655–663.

18. Carlsson M, Töger J, Kanski M, et al.: Quantification and visualization of cardiovascular 4D velocity mapping accelerated with parallel imaging or k-t BLAST: head to head comparison and validation at 1.5 T and 3 T. *J Cardiovasc Magn Reson* 2011; 13:55.

19. Busch J, Vannesjo SJ, Barmet C, Pruessmann KP, Kozerke S: Analysis of temperature dependence of background phase errors in phase-contrast cardiovascular magnetic resonance. *J Cardiovasc Magn Reson* 2014; 16:97.

20. Shadden SC, Dabiri JO, Marsden JE: Lagrangian Analysis of fluid transport in empirical vortex ring flows. *Phys Fluids* 2006; 18:047105.

21. Kramer CM, Barkhausen J, Flamm SD, Kim RJ, Nagel E, Society for Cardiovascular Magnetic Resonance Board of Trustees Task Force on Standardized Protocols: Standardized cardiovascular magnetic resonance (CMR) protocols 2013 update. *J Cardiovasc Magn Reson* 2013; 15:91.

22. Kheradvar A, Assadi R, Falahatpisheh A, Sengupta PP: Assessment of Transmitral Vortex Formation in Patients with Diastolic Dysfunction. *J Am Soc Echocardiogr* 2012; 25:220–227.

23. Nagueh SF, Appleton CP, Gillebert TC, et al.: Recommendations for the evaluation of left ventricular diastolic function by echocardiography. *J Am Soc Echocardiogr* 2009; 22:107–33.

24. Crapo RO, Casaburi R, Coates AL, et al.: ATS statement: Guidelines for the six-minute walk test. *Am J Respir Crit Care Med* 2002:111–117.

25. Töger J, Carlsson M, Söderlind G, Arheden H, Heiberg E: Volume Tracking: A new method for quantitative assessment and visualization of intracardiac blood flow from three-dimensional, time-resolved, three-component magnetic resonance velocity mapping. *BMC Med Imaging* 2011; 11:10.

26. Didden N: *Untersuchung Laminarer, Instabiler Ringwirbel Mittels Laser-Doppler-Anemometrie*. Göttningen: Max-Planck-Institut für Strömungsforschung; 1977.

27. Liess C: *Experimentelle Untersuchung Des Lebenslaufes von Ringwirbeln*. Göttningen: Max-Planck-Institut für Strömungsforschung; 1978.

28. Brecher GA: Critical Review of Recent Work on Ventricular Diastolic Suction. *Circ Res* 1958; 6:554–566.

29. Arvidsson PM, Töger J, Heiberg E, Carlsson M, Arheden H: Quantification of left and right atrial kinetic energy using four-dimensional intracardiac magnetic resonance imaging flow measurements. *J Appl Physiol* 2013; 114:1472–81.

30. Waters E a, Bowman AW, Kovács SJ: MRI-determined left ventricular “crescent effect”: a consequence of the slight deviation of contents of the pericardial sack from the constant-volume state. *Am J Physiol Heart Circ Physiol* 2005; 288:H848–H853.

31. Rich MW, Stitziel NO, Kovács SJ: Prognostic value of diastolic filling parameters derived using a novel image processing technique in patients > or = 70 years of age with congestive heart failure. *Am J Cardiol* 1999; 84:82–86.

32. Irisawa H, Wilson MFM, Rushmer RFR: Left ventricle as a mixing chamber. *Circ Res* 1960; 8:183–187.

33. Seo JH, Mittal R: Effect of diastolic flow patterns on the function of the left ventricle. *Phys Fluids* 2013; 25:110801.

34. Domenichini F: Three-dimensional impulsive vortex formation from slender orifices. *J Fluid Mech* 2011; 666:506–520.

35. Pedrizzetti G: Vortex formation out of two-dimensional orifices. *J Fluid Mech* 2010; 655:198–216.

36. Pasipoularides A, Vlachos PP, Little WC: Vortex Formation Time is Not an Index of Ventricular Function. *J Cardiovasc Transl Res* 2015; 8:54–58.

37. Shadden SC, Katija K, Rosenfeld M, Marsden JE, Dabiri JO: Transport and stirring induced by vortex formation. *J Fluid Mech* 2007; 593:315–331.

TABLES

Table 1. Subject characteristics.

	Controls (n=23)	Patients (n=23)
Age (years)	28±6	67±8 ***
Gender	10M, 13F	19M, 4F *
Weight (kg)	72±14	84±13 **
Length (cm)	176±11	178±8
BSA (m^2)	1.87±0.24	2.03±0.19 *
HR (bpm)	65±8	64±9
ESV (ml)	71±15	274±116 ***
DV (ml)	158±32	337±118 ***
EDV (ml)	178±32	364±116 ***
EDV/BSA (ml/m^2)	95±9	180±59 ***
SV (ml)	107±21	90±22 **
EWV_{Cine} (ml)	87±20	61±24 ***
EF	60±4%	26±8% ***
VFR	4.5±1.2	3.2±1.6 **
Mitral valve D (mm)	29±3	30±5

ESV = End-systolic volume, DV = diastatic volume, (see Figure 2), EDV = End-diastolic volume, EF = ejection fraction. HR = resting heart rate. SV = stroke volume, EWV_{Cine} = E-wave volume, (DV–ESV, Figure 2), BSA = Body surface area. VFR = vortex formation ratio (VFT, vortex formation time (2)). Values given as mean ± standard deviation.

*: $p<0.05$, **: $p<0.01$, ***: $p<0.001$ difference between controls and patients.

Table 2. Patient characteristics (n=23).

Etiology	
Ischemic	15/23 (65%)
Non-ischemic	8/23 (35%)
Diastolic dysfunction	
Impaired relaxation	6 (26%)
Pseudonormal	9 (39%)
Restrictive	5 (22%)
Could not be determined	3 (13%)
Blood pressure[a)]	
Mean systolic / diastolic	128±22 / 76±12
Hypertension	6/23 (26%)
ECG	
Mean QRS duration	158±31 ms
QRS duration ≥ 120 ms	21/23 (91%)
LBBB	21/23 (91%)
Medications	
ACE inhibitors	15/23 (65%)
ARB	6/23 (26%)
Beta blockers	20/23 (87%)
Diuretics	18/23 (78%)
Spironolactone	8/23 (35%)
Mitral regurgitation[b)]	

Mean	17±15%
<20%	14/23 (61%)
20%-50%	7/23 (30%)

a) Blood pressure taken on same day as CMR examination. In one patient, blood pressure at MR examination was not available. b) In two patients, 2D flow in the ascending aorta was not available or had insufficient image quality for quantification of mitral regurgitation.

Table 3. Quantitative mixing parameters in vivo (method 2) with interobserver and interstudy variability.

Controls (n=23)	VV (ml)	VV_{inflow} (ml)	VV_{mix-in} (ml)	MXR	VV_{mix-in}/ ESV	VV/DV
Observer 1	78±18	65±13	13±10	16±10%	18±12%	50±6%
Observer 2	76±19	66±13	10±11	11±11%	13±13%	47±7%
Interobserver variability	-2±7	1±3	-3±6	-4±8%	-5±10%	-2±5%
p-value (Wilcoxon)	0.092	0.28	0.023*	0.015*	0.016*	0.079
Patients (n=23)						
Observer 1	79±26	54±15	24±14	28±11%	10±6%	25±8%
Observer 2	75±26	56±16	19±13	23±13%	7±4%	23±7%
Interobserver variability	-3±9	1±3	-4±10	-5±9%	-2±4%	-2±7%
p-value (Wilcoxon)	0.075	0.06	0.04*	0.01**	0.015*	0.024*
Interstudy variability in controls (1.5T vs 3T, n=6)						
Observer 1, 3T	84±24	64±13	19±13	21±10%	25±13%	52±6%
Observer 1, 1.5T	86±26	61±16	25±13	28±9%	33±13%	53±8%
Interstudy variability	2±11	-4±9	6±5	7±5%	8±6%	1±7%
p-value (Wilcoxon)	0.67	0.37	0.044*	0.03*	0.031*	0.70*
Respiratory gating						

(1.5T Resp(+) vs Resp(-), n = 8)						
Observer 1, Resp(+)	74±20	63±16	12±7	16±9%	17±9%	47±4%
Observer 1, Resp(-)	70±18	65±18	5±6	6±10%	6±10%	44±6%
Difference	-5±10	3±6	-8±10	-9±11%	-9±12%	-2±6%
p-value (Wilcoxon)	0.26	0.31	0.059	0.06	0.076	0.28

VV = Vortex-ring volume, VVinflow = inflowing blood in vortex-ring, VVmix-in = blood mixed into the vortex ring, MXR = mixing ratio. Resp(+) and Resp(-) = 4D flow with respectively without respiratory gating. Values given as mean ± standard deviation. *: $p<0.05$, **: $p<0.01$. Bland-Altman plots are shown in Supporting Files 1-4.

FIGURES

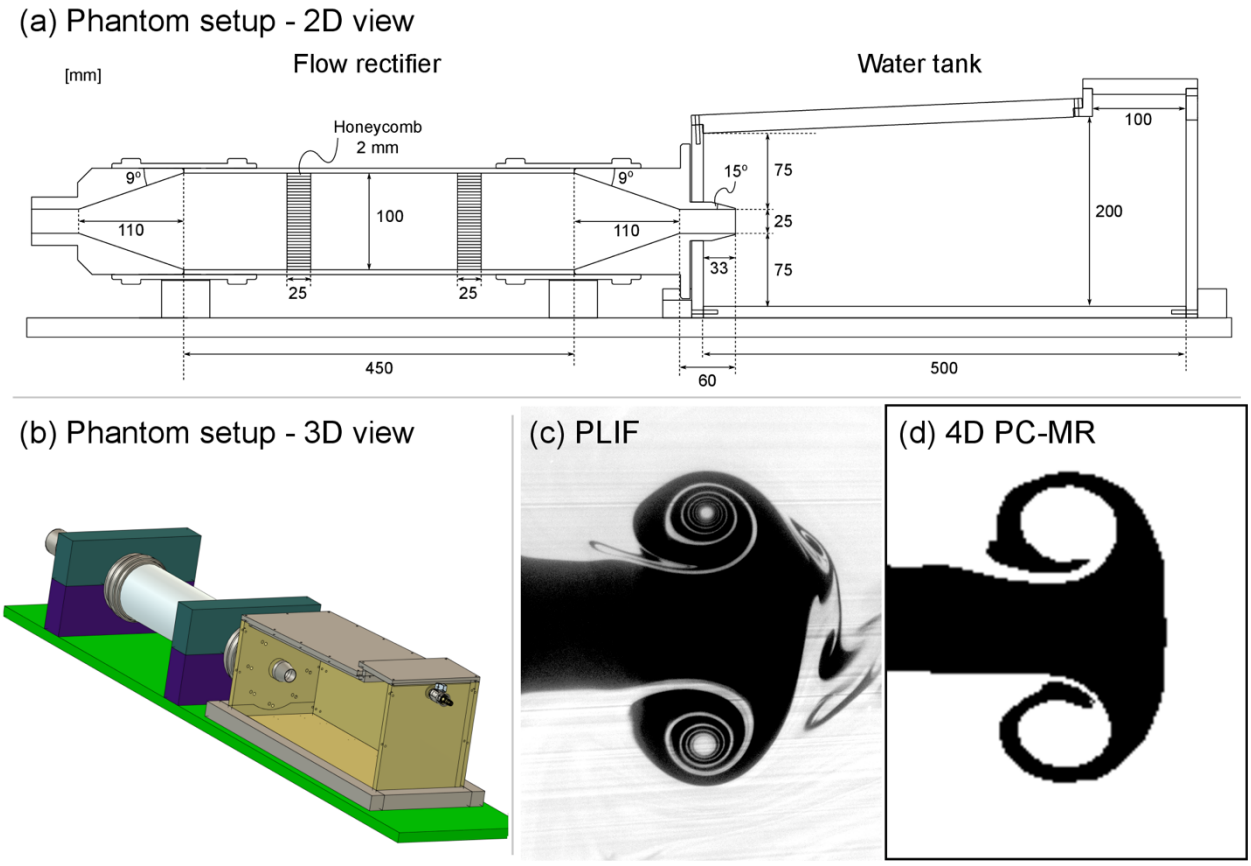

Figure 1: Phantom setup for validation of vortex-ring mixing ratio. Panels (a) and (b) show a schematic drawing of the phantom setup. Vortex-ring formation occurs at the 25 mm nozzle in the middle of the image (Panel a). Panel c shows a typical image of a vortex-ring using planar laser-induced fluorescence (PLIF). Panel d shows a corresponding particle tracing visualization of vortex-ring flow, measured using 4D flow.

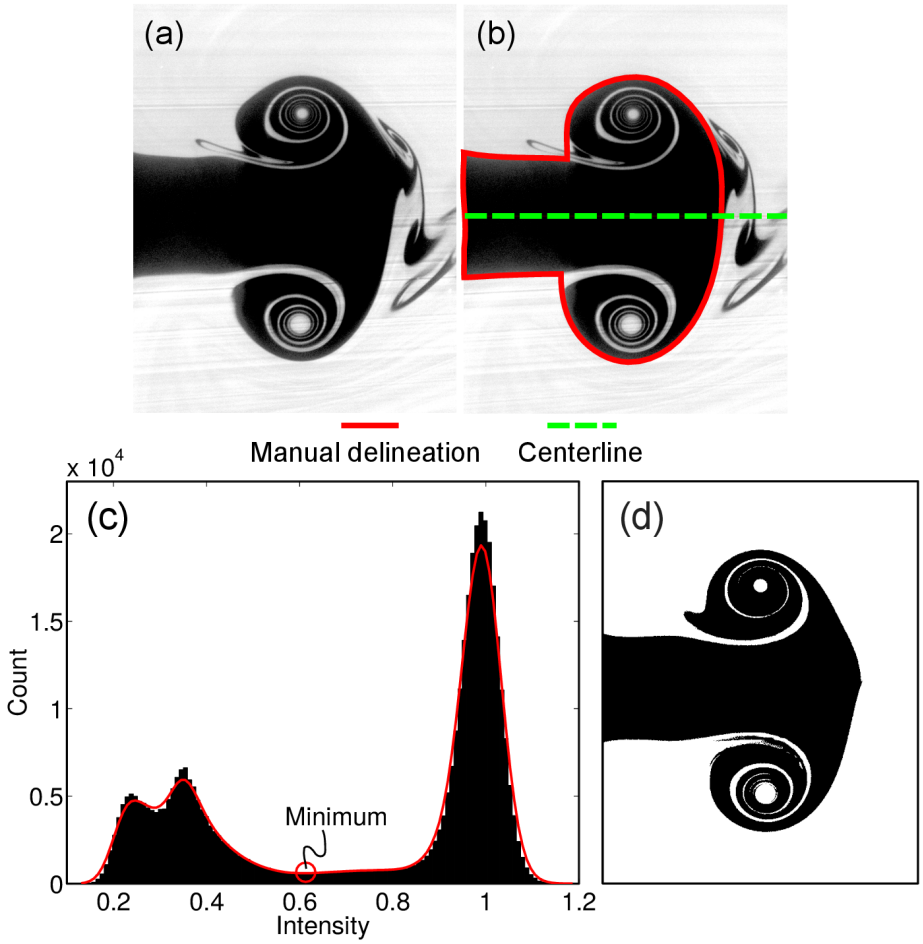

Figure 2: Phantom validation: analysis of MXR from PLIF images. Panel a: a PLIF image with applied intensity background correction. Panel b: manual delineation of the vortex-ring (red continuous line) and the computed centerline (green dashed line). Panel c: histogram of intensities in image pixels. The red line shows a Gaussian smoothing of the histogram. The red circle shows the minimum intensity between the last and second-to-last peaks, which defines the threshold between inflowing fluid (dark, below threshold) and fluid that was already in the tank before vortex-ring formation (white, above threshold). Panel d: resulting classification of each pixel in the vortex-ring.

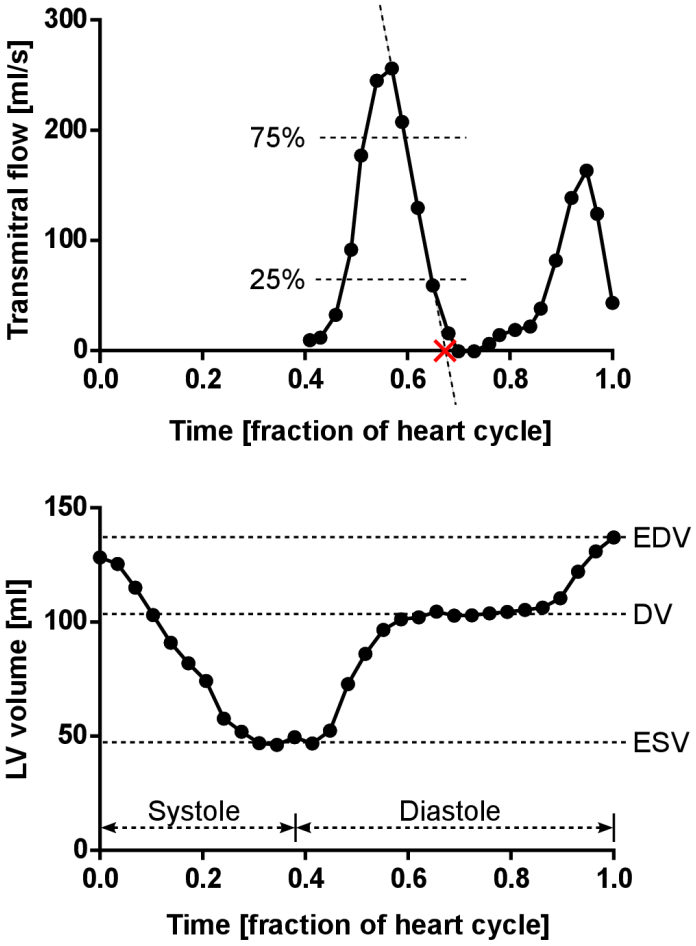

Figure 3: Definition of LV volumes and time phases. *Top:* Diastolic transmitral flow (ml/s) from one of the healthy volunteers. Early rapid filling (E) and diastasis (D) were determined from 4D flow quantification (solid line) in the left atrium. The slope between 25% and 75% of maximum flow during deceleration of rapid filling was extrapolated to zero to define the end of rapid filling. The red cross shows the time point where mixing analysis was performed. In cases where blood flow did not fall to 25% of peak flow, the time of minimal flow between the E and A peaks was used. In cases without diastasis (fusion of E- and A-waves), the 75% and 25% levels of the single filling peak were used.

Bottom: LV volume (ml) from one of the healthy volunteers during one cardiac cycle. Maximum LV volume defines the end-diastolic volume (EDV), and minimum LV volume defines the end-

systolic volume (ESV). Diastatic volume (DV) is the equilibrium volume at diastasis, after rapid filling but before atrial contraction. The E-wave volume (EWV_{Cine}), i.e. the LV volume increase during rapid filling, is defined by $EWV_{Cine}=DV–ESV$.

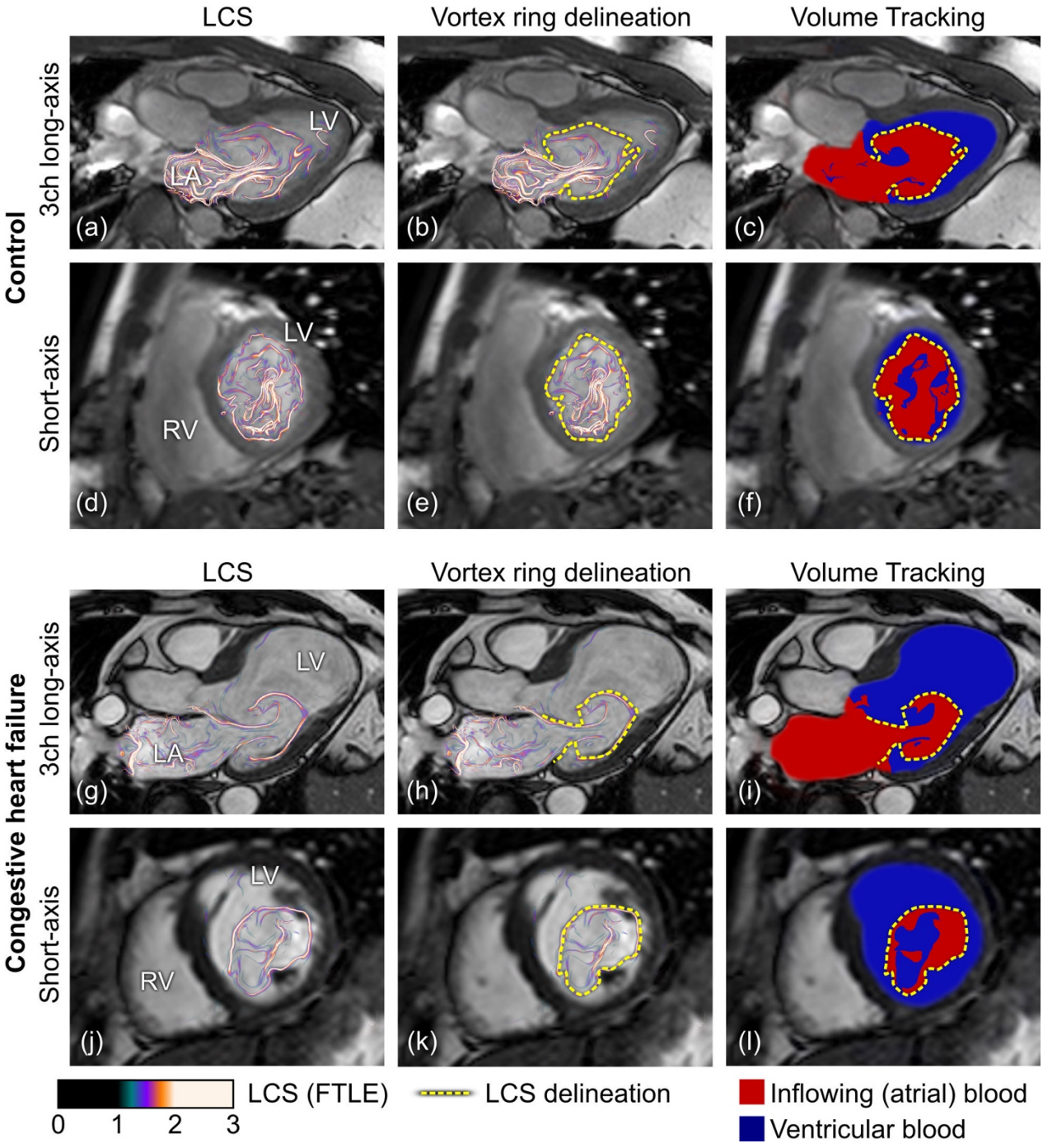

Figure 4: Mixing of blood during early rapid filling in a control (Panels a-f) and in a patient with congestive heart failure (Panels g-l). Blood flow visualization during early rapid filling of the LV, using Lagrangian Coherent Structures (LCS) and Volume Tracking (23), computed from 4D flow data. Left column (a,d,g,j): LCS. Middle column (b,e,h,k): Vortex-ring

boundary delineated from LCS (26). Since the trailing edge of the vortex-ring could not be observed, the leading edge was extrapolated towards the atrioventricular plane (see Limitations). Right column (c,f,i,l): Volume Tracking (23) visualization of inflowing blood (red) mixing with ventricular blood (blue). See Supporting Files 5 and 6 (online) for animated versions.

LA = left atrium, LV = left ventricle. FTLE = Finite-Time Lyapunov Exponent.

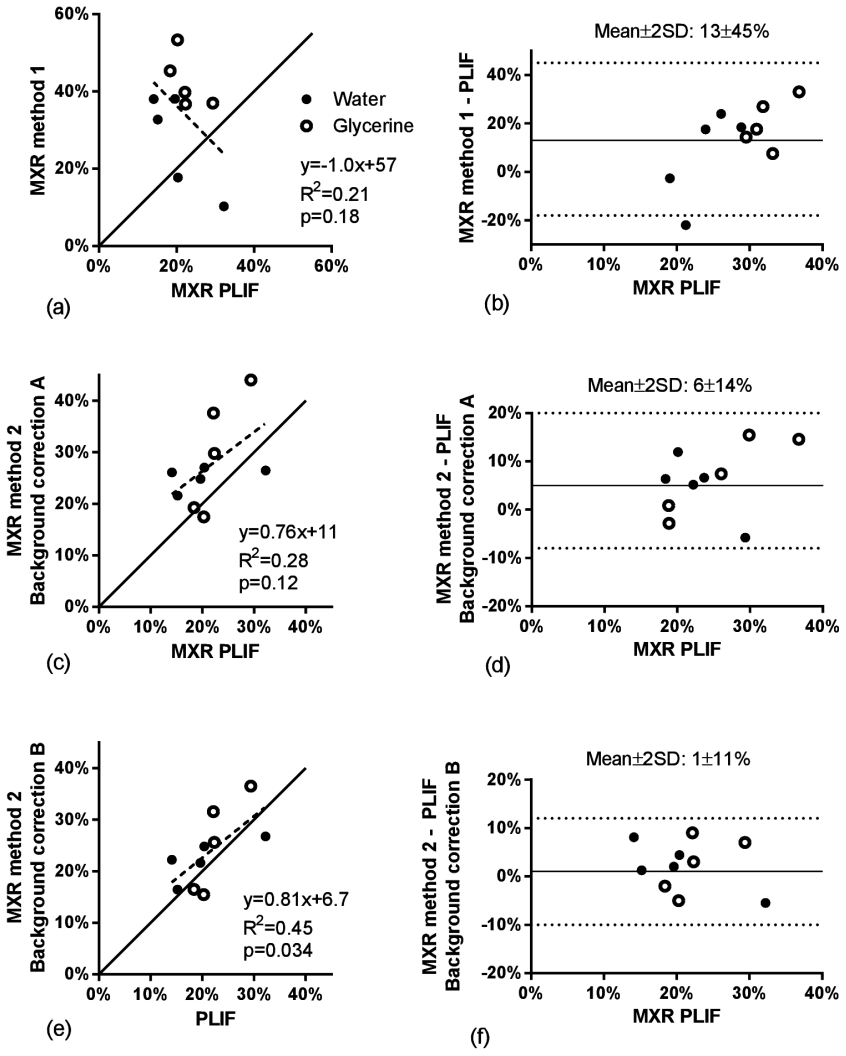

Figure 5: Phantom validation of 4D flow mixing ratio using PLIF as reference standard. Validation was performed using the phantom setup presented in Figure 1 (16). Panels a and b show results for MXR method 1. Poor accuracy and precision and a strong negative correlation were found. Panels c and d show MXR method 2 using background correction method A, which shows better agreement. Panels e and f show MXR method 2, with 4D flow background correction by subtraction of a stationary phantom scan (method B), which shows fair agreement between 4D flow and PLIF.

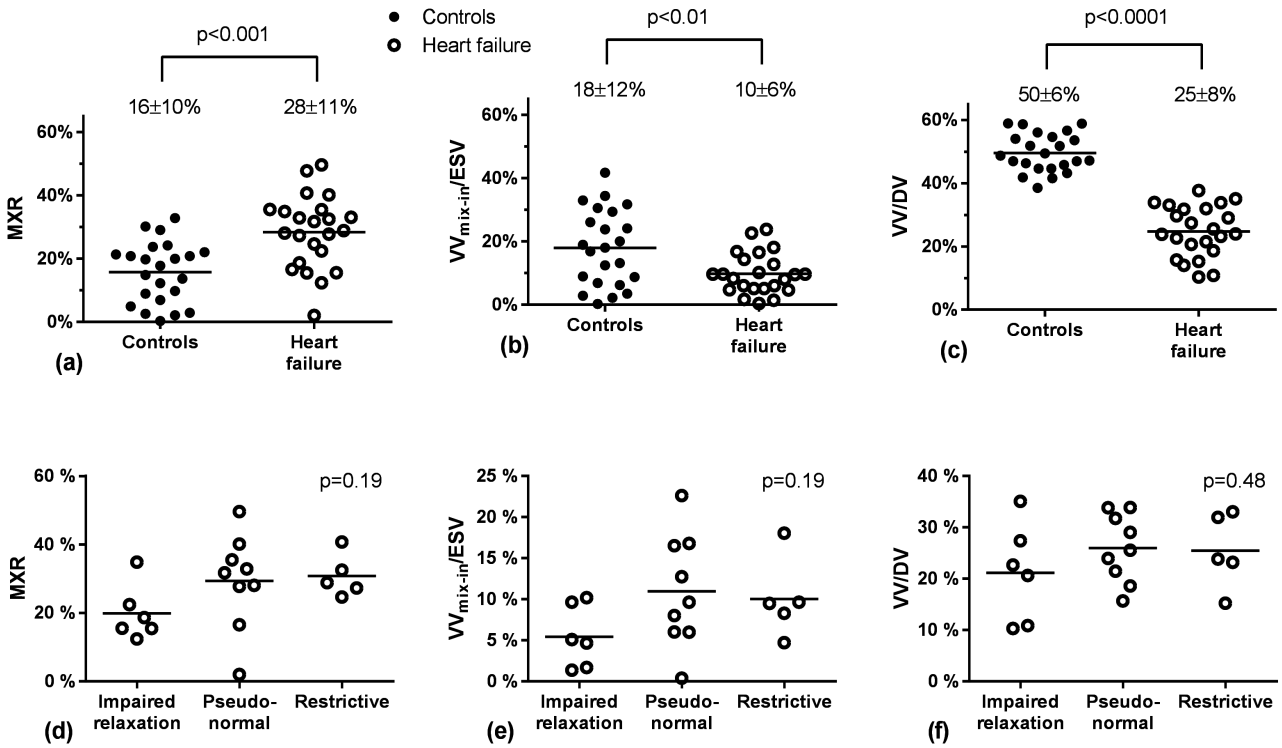

Figure 6: Quantitative mixing results. Panels a, b and c show a comparison of quantitative results for MXR, $VV_{mix\text{-}in}$ and VV/DV respectively in controls and patients with heart failure. Panels d, e and f show quantitative results for heart failure patients, divided by class of diastolic dysfunction. P-values in a, b and c: unpaired t-test. P-values in panels d, e and f: One-way ANOVA. Further results including interobserver and interstudy variability are shown in Table 3. Values are given as mean ± standard deviation.

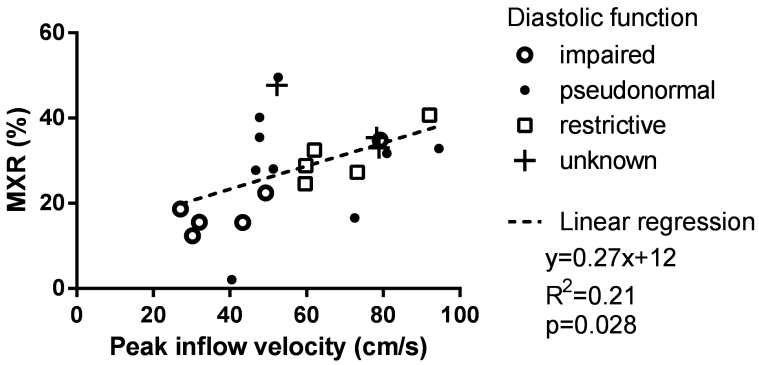

Figure 7: Scatter plot of peak diastolic inflow velocity and MXR. A moderate relationship was found, suggesting a connection between MXR and diastolic function.